ERROR ANALYSIS OF VISUAL ODOMETRY FOR A SMALL SIZE UNMANNED AERIAL VEHICLE

Önder Halis Bettemir[1]

[1] Department of Civil Engineering, İnönü University, Turkey, onder.bettemir@inonu.edu.tr

KEY WORDS: Unmanned Aerial Vehicle, Georeferencing, Accuracy, Error Propagation Law, Visual Odometry.

ABSTRACT:

Usage of small size Unmanned Aerial Vehicle (UAV) with autonomous flight capability became widespread at both civil and military applications because of its low costs and ease of use. However, inertial or GPS based positioning and orientation sensors can be disabled at battlefields and the UAV losses its path in a short time. Visual odometry becomes a solution for the aforementioned hassle. Real-time detection of ground control points, matching the same control points at the stereo pair images and correcting the position and orientation data with least square adjustment are the challenges of visual odometry. In this study, error analysis of position and orientation of a UAV flying through mountainous region which cannot obtain any augmenting data for position and orientation is conducted by error propagation law. The flight of UAV is simulated with exact initial position and orientation data. Optic images of ground obtained by nadir directed camera are georeferenced using the digital elevation model of the region, interior and exterior camera parameters. The digital elevation model is used to correct the relief displacement. The stereo-pair image is obtained when the UAV flies 200 m and image coordinates of the common control points are detected by colinearity equations. Position and orientation of UAV is corrected by least square adjustment and the process is repeated for each obtained image acquired at 200 m interval. The analysis revealed that the precisions of horizontal and vertical positioning becomes 75 and 200 meter, respectively. The precision of roll angle becomes worse than 0.5 degree, while the precisions of pitch and yaw angle are estimate to be better that 0.1 degree.

1. INTRODUCTION

Unmanned Aerial Vehicles (UAV) has many civil and military applications. Especially UAV swarms have significant impact on military tasks as UAVs are low cost and difficult to identify. On the other hand, the opponent can easily neutralize the UAV swarm by broadcasted jamming signal which deactivates the global positioning system or its remote control system. Positioning accuracy of Inertial Navigation System (INS) declines as the small errors of acceleration and orientation measurements accumulates and ends up with important positioning errors (Woodman, 2007; Rone and Ben-Tzvi, 2013; Wang et al., 2014). Therefore expensive INS components should be assembled to reduce the positioning error which eliminates the low cost advantage of UAV swarm. Visual odometry (VO) becomes an alternative for the positioning component as it does not require receiving any signal or data from the outside. Nistér et al. (2004) proposed a visual odometry algorithm based on stereo vision. In the literature important civil applications of VO exists (Aqel et al., 2016; Scaramuzza and Fraundorfer, 2011; Yousif et al., 2015; He et al., 2020). Forster et al (2014) reduced the requirement of pixel matching between the stereo images and obtained important amount of savings in terms of computational demand. Kaess et al. (2009) developed a visual odometry algorithm based on stereo vision. The algorithm was suitable for outdoor navigation and the key point was the parallax of the objects where objects placed at further would move less than the objects which are closer to the camera at consecutive images. Konolige et al. (2010) emerged IMU data with stereo vision and tested the algorithm at outdoor. The vehicle traversed 10 km and better than 10 meter precision is obtained. Augmenting data has important advantages in visual odometry so that Levin and

Szeliski (2004) obtained successful results when they merged a low accuracy map of the terrain with the visual odometry data. The extracted features are correlated with map and the accuracy of the visual odometry is improved. Konda and Memisevic (2015) developed a Convolutional Neural Network Algorithm to detect changes in camera attitude and velocity. The neural network is trained by KITTI Vision benchmark data set (Geiger et al., 2012). The neural network is trained by 500,000 data sets whose dimensions are reduced by principal component analysis. The proposed approach did not provide accurate results when compared with the results of the state-of-the-art methods and algorithms. In addition to this, the computational demand of the neural network is so demanding that graphical processing unit is utilized to conduct the computations. Nonetheless, the utilized deep learning based methodology had the potential of providing robust results as the neural network based methods have important capabilities.

Many VO applications have stereo vision as the vehicle moves on land. However, the distance between the vehicle and the ground can be very long when compared with the base distance of the stereo cameras which dilutes the stereo effect. Therefore, monocular VO is more suitable for UAV.

Georeferencing of optic images are examined comprehensively in the literature (Teppati et al., 2020). Štroner et al. (2021) abridged the relief displacement by obtaining multi images at various heights which improved the precision of the georeferencing (Štroner et al., 2021). Liu et al. (2022) produced directly georeferenced images with 4 cm RMSE in the horizontal direction by bundle adjustment (Liu et al, 2022). Štroner et al. (2020) utilized structure from motion algorithm and combined the algorithm with ground control points to

strengthen the output of the method. It is stated that at least one ground control points should be incorporated to obtain satisfactory results. Similar approach is conducted by Przybilla et al., (2020) to produce accurately georeferenced images. Introducing 1 ground control point for each georeferencing task provides important improvements while the accuracy of georeferencing decreases to 30 Ground Sample Distance (GSD) if ground control points are not utilized. Accurate georeferencing of satellite images without Ground Control Points can be achieved as long as excellent positioning and attitude detection devices are utilized (Bettemir, 2011a).

Literature review represent that the utilization of Ground Control Points have important effect on the success of the georeferencing. However, utilizing a ground control point for the georeferencing of optical images at a combat field is almost impossible. Therefore, visual odometry based position and attitude detection tasks have to be executed without ground control points. In this study precision of the position and orientation of a UAV is estimated by simulating its flight on a mountainous region. The error estimation of a UAV with monocular VO is performed recently (Bettemir, 2023). The established flight simulation and resection models have high correlations which causes important numeric errors during matrix inversions. In this study, the flight model and resection equations are rearranged to reduce the numerical problems which can be the contribution of this study.

In the following part of the manuscript, equations and the algorithm of the error estimation of visual odometry are introduced in detail. The implementation details and the simulation process are exemplified in the results part where a case study is conducted. Then the results and findings of the implemented methods are discussed. In addition to this, the contribution of the study and possible future works are concluded in the final part.

2. METHOD

The proposed error analysis algorithm is based on the VO of a flying UAV which cannot receive any GPS signal and its inertial navigation unit is malfunctioning. The position and orientation of an on-board camera, so that the UAV is corrected by stereo-images obtained by monoscopic optic camera. Images obtained at nadir direction are georefererenced by utilizing the digital elevation model of the terrain. Stereo-images are formed by matching the overlapping images acquired at regular intervals. Camera position and attitude thus the Cartesian coordinates and Euler rotation angles of the UAV are corrected by parameter estimation process which utilizes the common ground points existing at the overlapping image regions. The corrected position and orientation has certain uncertainty since the common ground points cannot be matched perfectly and the georeferencing process has also some uncertainty. This study aims to predict the amount of uncertainty of a UAV navigated by visual odometry flying at a mountainous region. The ambiguity of the position and orientation is predicted by an error propagation law based algorithm. The aforementioned statistical technique was applied to predict the uncertainty of georeferencing of satellite images (Bettemir, 2006). Flowchart of the algorithm which estimates the uncertainty of positioning by visual odometry is given in Figure 1.

The algorithm utilizes the obtained images which are acquired at regular time intervals. Initial position, orientation, and velocity of the UAV are assumed to be precisely known. The

positioning sensors are assumed to be blinded at time t_0 and the vehicle starts dead reckoning by VO.
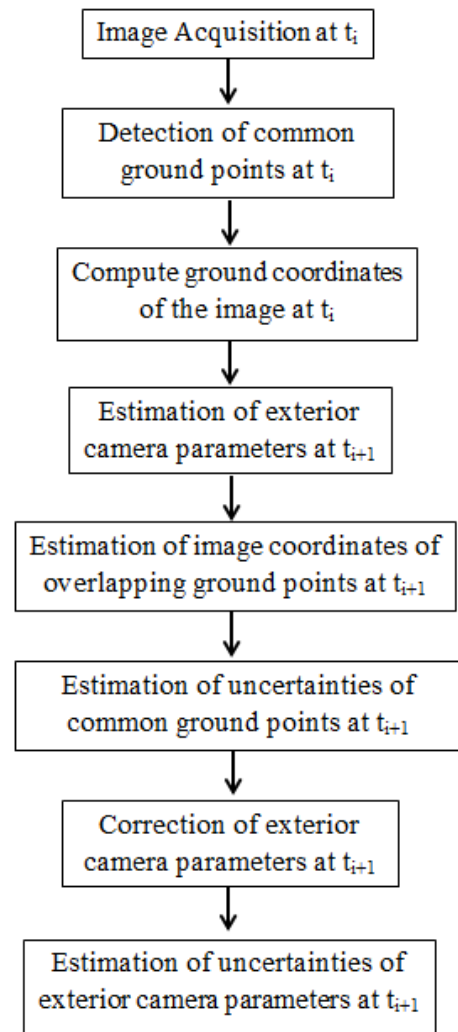

Figure 1. Flowchart of the error estimation algorithm of VO.

The first acquired image is georeferenced by the exactly known camera position and orientation without utilizing ground control points. Georeferencing is conducted by the colinearity equations given in Eq. 1 and 2 (Kraus, 1993).

$$X = X_0 + (Z - Z_0)$$
$$\left\{ \begin{bmatrix} 1 - k_1 * r^2 - k_2 * r^4 - 2p_1 x' - 2p_2 y' - \dfrac{p_1 r^2}{x'} \end{bmatrix} * \atop \begin{bmatrix} \dfrac{cR_{11}(x' - \Delta x) + cR_{12}(y' - \Delta y) - R_{13}f}{cR_{31}(x' - \Delta x) + cR_{32}(y' - \Delta y) - R_{33}f} \end{bmatrix} \right\} \quad (1)$$

$$Y = Y_0 + (Z - Z_0)$$
$$\left\{ \begin{bmatrix} 1 - k_1 * r^2 - k_2 * r^4 - 2p_1 x' - 2p_2 y' - \dfrac{p_2 r^2}{y'} \end{bmatrix} * \atop \begin{bmatrix} \dfrac{cR_{21}(x' - \Delta x) + cR_{22}(y' - \Delta y) - R_{23}f}{cR_{31}(x' - \Delta x) + cR_{32}(y' - \Delta y) - R_{33}f} \end{bmatrix} \right\} \quad (2)$$

In Eq. 1 and 2 R_{ij} expressions are the elements of the Euler rotation matrix which is formed by the roll, pitch and yaw angles of the camera. The rotation matrix is given below.

$$\begin{bmatrix} \cos\phi\cos\kappa & -\cos\phi\sin\kappa & \sin\phi \\ \sin\omega\sin\phi\cos\kappa + \cos\omega\sin\kappa & -\sin\omega\sin\phi\sin\kappa + \cos\omega\cos\kappa & -\sin\omega\cos\phi \\ -\cos\omega\sin\phi\cos\kappa + \sin\omega\sin\kappa & \cos\omega\sin\phi\sin\kappa + \sin\omega\cos\kappa & \cos\omega\cos\phi \end{bmatrix}$$

In Eq. 1 and 2, r represents the radial distance between the investigated pixel whose coordinates are x', y' and the principal point of the CCD array. Initially the distance is measured in pixel then the unit is converted to mm. Radial lens distortion parameters are represented by k_1 and k_2, decentering lens distortion is corrected by parameters which are p_1 and p_2. f is the focal length of the camera; c is the size of the sensing element on the CCD frame; principal coordinate of the camera is expressed by Δx and Δy parameters whose unit is pixel. Cartesian camera coordinate is shown by X_0, Y_0 and Z_0 parameters in mm. Position of ground point is also represented in Cartesian coordinate with three parameters where Z expresses the elevation of the ground point. Horizontal position is expressed by X and Y parameters.

Initially elevations of the ground points are not known and Eq. 1 and 2 have infinite number of feasible solutions of horizontal coordinates with respect to different elevation value. Relief displacement is corrected by an iterative process which utilizes digital elevation model (DEM) of the terrain. Initially, the ground elevation is assumed to be 1000 meter and this value is checked from the loaded DEM by using the computed X and Y ground coordinates. Eqs. 1 and 2 are implemented again to compute the horizontal ground coordinates and corrected elevation is obtained from DEM using the updated horizontal coordinates if the difference between the obtained elevation and the utilized elevation is more than 0.1 meters. This process is repeated until the elevation difference is reduced below 0.1 meter. This step constitutes the computation of ground coordinates at t_i. Aforementioned relief displacement process requires at most four iterations satisfy the stopping criteria (Bettemir, 2011b).
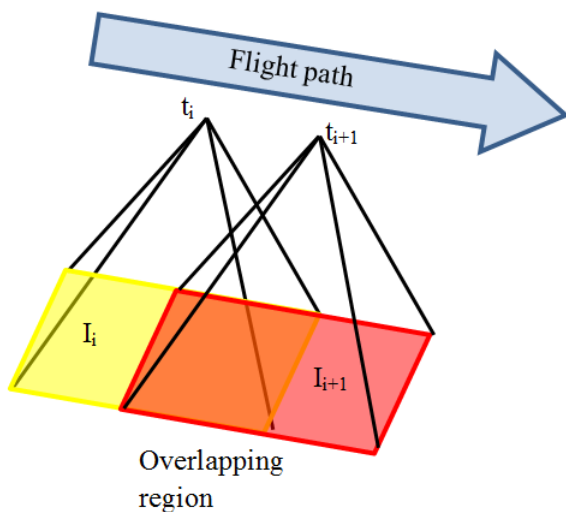
Figure 2. Illustration of flight direction and the imaging sequence.

UAV acquires optic images at regular intervals where subsequent images overlap. Common ground points with sharp edges are detected on the image autonomously and their ground coordinates are obtained. Camera position and attitude of event $i + 1$ is estimated by the current position and velocity vectors.

In this step random errors are added to camera position and orientation. The obtained parameters are corrected by resection. The imaging sequence shown in Figure 2 provides overlapping images and enables detection of common ground points. Common ground points which are at the overlapping regions of the images acquired at event i and $i + 1$ are detected and their estimated image positions at I_{i+1} is computed by using their ground coordinates and the updated camera coordinates. The detected points on the image I_{i+1} are used for the correction of camera attitude and orientation. Coordinates of the common ground points are known by the georeferencing of the image I_i. The pixel coordinates of the common ground points are also known for the image I_{i+1}. The image coordinates of the common ground points are computed by Eq. 3 and 4 (Karara, 1989) although they are already known.

$$x = \Delta X - f/c *$$
$$\left\{ \left[\frac{R_{11}(X-X_0) + R_{21}(Y-Y_0) - R_{31}(Z-Z_0)}{R_{13}(X-X_0) + R_{23}(Y-Y_0) - R_{33}(Z-Z_0)} \right] \right\} \quad (3)$$

$$y = \Delta Y - f/c *$$
$$\left\{ \left[\frac{R_{12}(X-X_0) + R_{22}(Y-Y_0) - R_{32}(Z-Z_0)}{R_{13}(X-X_0) + R_{23}(Y-Y_0) - R_{33}(Z-Z_0)} \right] \right\} \quad (4)$$

Image coordinates computed by Eq. 3 and 4 are expected to be different with the exact image coordinates determined by correlating the overlapping regions. The computed image coordinates differ because of the error of the position and uncertainty. This leads to an inconsistency between the image position and ground position computed by Eq. 3 and 4. Parameter estimation is performed by least square adjustment to correct the exterior camera parameters of event i+1. Least square adjustment formulation implemented in this study is given in Eq. 5 (Koch, 1999).

$$\Delta\beta = \left(X^T X\right)^{-1} X^T \Delta y \quad (5)$$

In Eq. 5 Δy is the differences between of the image coordinates obtained by executing Eq. 3 to 4 and image correlation. In this study the exact image coordinates are obtained by utilizing the exact exterior camera position and attitude and utilizing Eq. 3 to 4. $\Delta\beta$ is the computed corrections for the exterior camera parameters. X is the matrix which includes the partial derivatives of the colinearity equations given in Eq. 3 and 4 taken with respect to camera position and camera attitude. The partial derivative equations of the exterior camera parameters at event $i + 1$ are computed according to the image I_i. Formation of X matrix is given in Eq. 6.

$$X = \begin{bmatrix} \dfrac{\partial x_1}{\partial X_0} & \dfrac{\partial x_1}{\partial Y_0} & \dfrac{\partial x_1}{\partial Z_0} & \dfrac{\partial x_1}{\partial \omega} & \dfrac{\partial x_1}{\partial \phi} & \dfrac{\partial x_1}{\partial \kappa} \\[2mm] \dfrac{\partial y_1}{\partial X_0} & \dfrac{\partial y_1}{\partial Y_0} & \dfrac{\partial y_1}{\partial Z_0} & \dfrac{\partial y_1}{\partial \omega} & \dfrac{\partial y_1}{\partial \phi} & \dfrac{\partial y_1}{\partial \kappa} \\[2mm] \dfrac{\partial x_2}{\partial X_0} & \dfrac{\partial x_2}{\partial Y_0} & \dfrac{\partial x_2}{\partial Z_0} & \dfrac{\partial x_2}{\partial \omega} & \dfrac{\partial x_2}{\partial \phi} & \dfrac{\partial x_2}{\partial \kappa} \\[2mm] \dfrac{\partial y_2}{\partial X_0} & \dfrac{\partial y_2}{\partial Y_0} & \dfrac{\partial y_2}{\partial Z_0} & \dfrac{\partial y_2}{\partial \omega} & \dfrac{\partial y_2}{\partial \phi} & \dfrac{\partial y_2}{\partial \kappa} \\[2mm] \vdots & \vdots & \vdots & \vdots & \vdots & \vdots \\[2mm] \dfrac{\partial x_n}{\partial X_0} & \dfrac{\partial x_n}{\partial Y_0} & \dfrac{\partial x_n}{\partial Z_0} & \dfrac{\partial x_n}{\partial \omega} & \dfrac{\partial x_n}{\partial \phi} & \dfrac{\partial x_n}{\partial \kappa} \\[2mm] \dfrac{\partial y_n}{\partial X_0} & \dfrac{\partial y_n}{\partial Y_0} & \dfrac{\partial y_n}{\partial Z_0} & \dfrac{\partial y_n}{\partial \omega} & \dfrac{\partial y_n}{\partial \phi} & \dfrac{\partial y_n}{\partial \kappa} \end{bmatrix} \tag{6}$$

Similarly Δβ is shown in Eq. 7.

$$\Delta\beta = \begin{bmatrix} \Delta X_0 \\ \Delta Y_0 \\ \Delta Z_0 \\ \Delta \omega \\ \Delta \phi \\ \Delta \kappa \end{bmatrix} \tag{7}$$

The colinearity equations are not continuous thus differentiable because of relief displacement process. Therefore, partial derivatives are computed by numeric derivative. In order to compute the numeric derivative accurately, function values obtained at five-points are considered. The numerical derivative is given in Eq. 8 (Abramowitz, 1972).

$$f'(x) = \frac{-f(x+2h) + 8f(x+h) - 8f(x-h) + f(x-2h)}{12h} \tag{8}$$

In Eq. 8, h is the step size of the numeric derivative. In this study, h is taken as one millionth of the value of the parameter.

Corrections are added to the camera position and orientation at the end of each space resection task and the corrected exterior camera parameters are obtained as shown in Eq. 9.

$$\begin{bmatrix} \hat{X}_0 \\ \hat{Y}_0 \\ \hat{Z}_0 \\ \hat{\omega} \\ \hat{\phi} \\ \hat{\kappa} \end{bmatrix}_i = \Delta\beta + \begin{bmatrix} X_0 \\ Y_0 \\ Z_0 \\ \omega \\ \phi \\ \kappa \end{bmatrix}_i \tag{9}$$

Correction of the exterior camera parameters finishes the ith imaging step. The process continues by following the aforementioned steps until the vehicle reaches its destination. Variance of the estimated parameters is computed as given in Eq. 10.

$$\mathrm{var}(\beta) = \sigma^2 \left(X^T X \right)^{-1} \tag{10}$$

Where

$$\sigma^2 = \frac{S}{n-m}$$

S is the sum of the square of the residuals, n − m is the statistical degree of freedom. In this study number of estimated parameters, m, is 6 and n is the number of observations. Computation of the variance of the parameters is the scope of this study which gives an idea of the uncertainty of the position and attitude of the UAV. The aforementioned process is programmed in MatLAB software.

3. RESULTS

Proposed uncertainty estimation of exterior camera parameters is implemented in order to detect the suitability of the algorithm. Case study aims to detect any numeric problems that can encountered throughout the computation process. The UAV flew 4000 meters over a mountainous region by taking optical images with 200 meter intervals. The flight speed is assigned as 40 m/s which lead to 5 seconds imaging interval. Randomly distributed 20 common ground points are assumed to be detected at the overlapping portion of the images.

Interior parameters of the camera obtained by a camera calibration process are given in Table 1. The optic camera is a mass produced low price DSLR type and can be obtained easily. Small UAVs which have at most 1 kg take-off weight can carry the mentioned payload. The camera has 0.8 MP charged coupled device array.

| Parameter	Value	Unit
f	55	mm
c	0.017	mm
Δx	35	Pixel
Δy	5.5	Pixel
k_1	2.0×10^{-5}	$1/mm^2$
k_2	2.0×10^{-16}	$1/mm^4$
p_1	2.0×10^{-10}	$1/mm^2$
p_2	2.0×10^{-10}	$1/mm^2$

Table 1. Utilized interior camera parameters for the case study.

Randomly generated terrain is formed in order to form steep slopes and high elevation differences throughout the terrain. A quadratic polynomial is adopted to generate the terrain whose plot is shown in Figure 3.

Minimum elevation of the terrain is 500 meters, while the maximum elevation is 924. The mentioned elevation difference is experienced five times during a 4 km flight. Therefore, the terrain can be considered as a mountainous region. Flight altitude is set as 3800 meters. Position and attitude values are set as given in Table 2 at the beginning of the flight.

Parameter	Value
X_0	500
Y_0	1600
Z_0	3800
ω	0
φ	0
κ	0

Table 2. Initial exterior camera parameters for the case study.
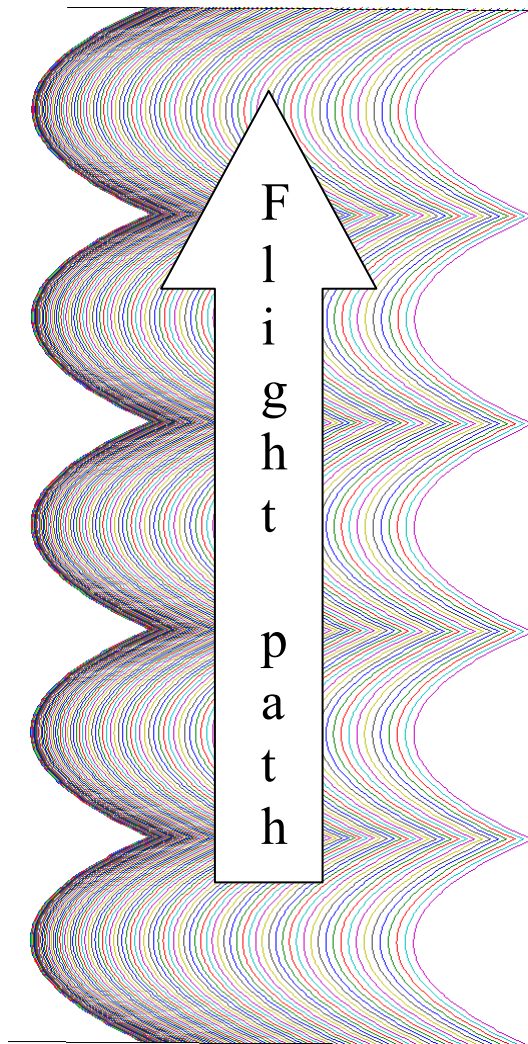
Figure 3. Randomly generated terrain.

The vertical distance between the ground surface and the aerial vehicle differs between 3300 and 2864 meters. The assigned exterior and interior camera parameters lead to the ground resolution presented below.

$$resolution_{max} = \frac{c}{f} * h_{min}$$

$$resolution_{max} = \frac{0.017}{55} * 2864 = 0.885m$$

$$resolution_{min} = \frac{c}{f} * h_{max}$$

$$resolution_{min} = \frac{0.017}{55} * 3300 = 1.020m$$

Provided maximum and minimum values occur at the same image at every image acquisition which leads to important magnitude of relief displacement within the image. This makes the important relative displacements among the common ground points.

Camera coordinates are given at local coordinate system in which the altitude is the mean sea level. Initial flight direction is through the positive x axis. The UAV aims to move 4000 m in x direction without changing the Y and Z coordinates. Obtained variance-covariance matrix is presented for each 1000 meter flight.

The matrix representing the uncertainty of the camera position and attitude measured after 1000 meter flight is presented in Table 3.

	X	Y	Z	ω	φ	κ
X	97,72	-1,35	21,26	1,91E-08	1,91E-08	1,91E-08
Y	-1,35	0,09	-0,38	1,44E-10	1,44E-10	1,44E-10
Z	21,26	-0,38	6,39	4,66E-09	4,66E-09	4,66E-09
ω	0,00	0,00	0,00	0	0	0
φ	0,00	0,00	0,00	0	0	0
κ	0,00	0,00	0,00	0	0	0

Table 3. Variance-covariance matrix obtained after the first 1000 meter flight.

Table 3 represents that the Cartesian coordinates of the camera has lost its accuracy especially for the X direction. The elevation measurements are also deteriorated but it is not as much as the deterioration of the X coordinates. Moreover, correlations of the X coordinate with other parameters also significant. Variances of the attitude parameters are shown as zero but they are in the order of E-17 and they are rounded to zero. Variance-covariance matrix of the second 1000 meter is shown in Table 4.

	X	Y	Z	ω	φ	κ
X	103,67	-2,65	29,41	1,50E-08	1,50E-08	1,50E-08
Y	-2,65	0,12	-0,81	-3,01E-10	-3,01E-10	-3,01E-10
Z	29,41	-0,81	9,43	3,60E-09	3,60E-09	3,60E-09
ω	0,00	0,00	0,00	0	0	0
φ	0,00	0,00	0,00	0	0	0
κ	0,00	0,00	0,00	0	0	0

Table 4. Variance-covariance matrix obtained after the second 1000 meter flight.

Variance of the camera position does not increase significantly. The increase of the elevation and the correlation of elevation with X coordinate are noticeable. Moreover, the correlation of the camera attitude also increased when compared with the previous variance covariance matrix. Variance-covariance matrix of the third 1000 meter is not provided due to space limitation.

In the third step, variance of the camera position slightly improved which is contrary to expectations. When the topography is examined the given uncertainties are obtained just after the flat top of the artificial hill. This may end up with low relief displacement of ground points between consecutive images. Proper matching of the ground points is considered to improve the overall positioning accuracy. Variance-covariance matrix of the fourth 1000 meter is shown in Table 5.

	X	Y	Z	ω	φ	κ
X	102,89	-2,47	22,51	-3,29E-08	-3,29E-08	-3,29E-08
Y	-2,47	0,21	-0,83	-1,52E-10	-1,52E-10	-1,52E-10
Z	22,51	-0,83	7,55	-9,31E-09	-9,31E-09	-9,31E-09
ω	0,00	0,00	0,00	0,00	0,00	0,00
φ	0,00	0,00	0,00	0,00	0,00	0,00
κ	0,00	0,00	0,00	0,00	0,00	0,00

Table 5. Variance-covariance matrix obtained after the fourth 1000 meter flight.

In the fourth step it is seen that the precision of the camera coordinates are worse than the third cycle. This represents that the uncertainty of the camera position fluctuates during the flight with an overall increasing trend. Analysis are conducted on a laptop computer with 2,4 GHz i5 CPU in two seconds. The obtained accuracy is not satisfactory when the computational demand and flight distance are considered.

Simulation process is executed without numerical error which is a main contribution of this study when compared with the previous studies (Bettemir, 2023). Elimination of numerical errors also reduces the computational errors and increases the reliability of the results.

4. DISCUSSION AND CONCLUSION

In this study uncertainty of a UAV flying with only visual odometry is examined. In this special case, the UAV cannot receive any augmenting navigation data such as GPS positioning, gyroscope or accelerometer. The principle of navigation depends on the detection of common ground points from the overlapping region of the two consecutive images.

Proposed algorithm is simulated on a mountainous region and the expected positional precision is estimated by error propagation law based algorithm. The position and attitude of the UAV is corrected by space resection procedure which utilizes the ground coordinates of the common ground points that take part at the successive images. The space resection process is conducted with least square adjustment with matrix inversion. The ground points are selected by random distribution and a numeric problem is not observed through the simulation process. However, sometimes condition number of the matrix fell to 1E-20 which means the rounding error of the computer can be significant. Besides the aforementioned case no numerical error is observed during the computations.

The mean square error of the position of the UAV is estimated as 108 meters which is the norm of the variance covariance matrix. The simulation is repeated several times and similar matrix norms are obtained. This means that the proposed visual odometry algorithm provides ± 100 meters of precision after 4000 meters of flight over a mountainous region. The obtained precision is not enough for many autonomous flight applications which means that the proposed navigation algorithm should be improved.

Besides the mentioned incapability the proposed algorithm has some positive aspects. The proposed algorithm can provide the route without considering the initial velocity or any augmenting data. This means that the implemented visual odometry can be used as a standalone navigation technique after improving its overall precision.

In this simulation, 20 common ground points which properly covers the overlapping region are used for the parameter estimation process. The number of common ground points can be increased to improve the accuracy and dependability of the proposed algorithm. On the other hand, the proposed improvement requires ensuring the proper distribution of the common ground points in order to prevent singularity.

The algorithm can be improved by including different navigation data such as velocity of the UAV to roughly predict the camera position when the next image is acquired. Also deep learning based methods can be implemented to improve the accuracy of the matching of the common ground points. LIDAR based systems can improve the precision of elevation data. However, the proposed sensors integrations eliminate the economy of the method.

The algorithm is simulated in 2 seconds on a laptop computer. Flight duration of a small UAV would be more than three minutes to fly four kilometre distance which means that the algorithm can be run real-time on-board central processing unit of the UAV. However, computational demand of the algorithm should be decreased to prevent possible delays in real time applications.

Matching the common ground points at the consecutive images is a tedious and highly an error prone task because of the high possibility of mismatch of the picture elements. The success rate of matching the picture elements increases when the illumination is proper and the terrain is smooth. However at mountainous regions, the exposure angle of the ground point changes significantly when two successive overlapping images are compared. The aforementioned situation decreases the success of the pixel matching at mountainous region. In addition to this, snow cover on the terrain makes obtaining enough common ground points difficult as the pattern becomes similar.

The parameter estimation process can be strengthened by introducing Kalman Filter to reduce the uncertainty caused by the inconsistencies of the pixel positions located at the consecutive images. The discrepancy can be reduced and better results can be obtained by applying more endowed methods. The workload of Kalman Filter is more than least square adjustment but the additional computational demand can be handled by parallel processing algorithms to enable real time computation.

Uncertainty of position and orientation is also examined in te literature (Bettemir, 2013; 2009; 2010; 2023). Apart from Bettemir (2023) the utilized approach based on only one monoscopic image which does not require the computation of accumulating uncertainty. The model constructed by Bettemir 2023 was close to ill-conditioned system and computation of matrix inversions were reported to be near singular by the utilized MatLAB software. In this study, more efficient geometry is constructed and the Frobenius norm of the matrix to be inverted is improved. Therefore, the obtained results are more dependable then the previous studies.

In this study, precision of autonomous flight of a small low-price unmanned aerial vehicle is estimated by simulation. The precision estimation algorithm is based on error propagation

law; therefore the implemented algorithm requires computation of matrix inversion. Numerical derivatives to construct partial derivatives are obtained by numerical methods. The simulation executed without any numerical problems. The proposed visual odometry based navigation algorithm provided 108 meters of uncertainty after 4 kilometre of flight over a mountainous region. The accuracy of the proposed visual odometry based algorithm should be improved as a future study. Investigating the flight height, increasing the number of common ground points in the overlapping region can be promising. Moreover, the interval between the consecutive images can be examined substantially as a future study.

REFERENCES

Abramowitz M., Stegun I. A., 1972. *Handbook of Mathematical Functions With Formulas, Graphs, and Math. Tables*. New York: Dover.

Aqel, M. O., Marhaban, M. H., Saripan, M. I., Ismail, N. B. 2016. Review of visual odometry: types, approaches, challenges, and applications. *SpringerPlus*, 5, 1-26.

Bettemir, Ö. H. (2023, June). Sensitivity Analysis to Estimate the Positional Accuracy of a Small Size Unmanned Aerial Vehicle. *In 2023 10th International Conference on Recent Advances in Air and Space Technologies (RAST)* (pp. 1 - 6). IEEE.

Bettemir, Ö. H. 2011a. Prediction of georeferencing precision of pushbroom scanner images. *IEEE transactions on geoscience and remote sensing*, 50(3), 831-838.

Bettemir, Ö. H., June 2011b. Determination of optimum STC orientation by GA. *In Proceedings of 5th International Conference on Recent Advances in Space Technologies-RAST2011* (pp. 203-208). IEEE.

Bettemir, Ö. H. 2010. Error estimation of orthorectification of small satellite images by differential sensitivity analysis. *Journal of Aeronautics and Space Technologies*, 4(4), 65-74.

Bettemir, Ö. H. 2009, June. Differential sensitivity analysis for the orthorectification of small satellite images. *In 2009 4th International Conference on Recent Advances in Space Technologies* (pp. 386-391). IEEE.

Bettemir, Ö. H. 2006. Sensitivity and error analysis of a differential rectification method for CCD frame cameras and pushbroom scanners, *Master's thesis, Middle East Technical University*.

Forster, C., Pizzoli, M., Scaramuzza, D. 2014, May. SVO: Fast semi-direct monocular visual odometry. *In 2014 IEEE international conference on robotics and automation (ICRA)* (pp. 15-22). IEEE.

Geiger, A., Lenz, P., Urtasun, R. 2012. Are we ready for autonomous driving? The kitti vision benchmark suite. *In Conference on Computer Vision and Pattern Recognition (CVPR)*.

He, M., Zhu, C., Huang, Q., Ren, B., Liu, J. 2020. A review of monocular visual odometry. *The Visual Computer*, 36(5), 1053-1065.

Kaess, M., Ni, K., Dellaert, F. 2009: Flow separation for fast and robust stereo odometry. *In: IEEE International Conference on Robotics and Automation*, *2009* (ICRA'09), pp. 3539–3544.

Karara, M.H. 1989. *Non-topographic photogrammetry*. American society for photogrammetry and remote sensing.

Koch K. R., 1999. *Parameter estimation and hypothesis testing in linear models*, Second Edition Springer.

Konda, K. R., Memisevic, R. 2015. Learning visual odometry with a convolutional network. *VISAPP* (1), 2015, 486-490.

Konolige, K., Agrawal, M., & Sola, J. 2011. Large-scale visual odometry for rough terrain. *In Robotics Research: The 13th International Symposium ISRR* (pp. 201-212). Springer Berlin Heidelberg.

Kraus, K. Photogrammetry Volume 1 Fundamentals and Standard Processes, 4th Ed., *Dümmler*, Bonn, 1993.

Levin, A., Szeliski, R. 2004, June. Visual odometry and map correlation. *In Proceedings of the 2004 IEEE Computer Society Conference on Computer Vision and Pattern Recognition, 2004. CVPR 2004*. (Vol. 1, pp. I-I). IEEE.

Liu, X., Lian, X., Yang, W., Wang, F., Han, Y., Zhang, Y. 2022. "Accuracy assessment of a UAV direct georeferencing method and impact of the configuration of ground control points." *Drones*, 6(2), 30.

Nistér, D., Naroditsky, O., Bergen, J. 2004, June. Visual odometry. *In Proceedings of the 2004 IEEE Computer Society Conference on Computer Vision and Pattern Recognition*, 2004. CVPR 2004. (Vol. 1, pp. I-I). IEEE.

Štroner, M., Urban, R., Reindl, T., Seidl, J., Brouček, J. 2020. "Evaluation of the georeferencing accuracy of a photogrammetric model using a quadrocopter with onboard GNSS RTK". *Sensors*, 20(8), 2318,.

Przybilla, H. J., Bäumker, M., Luhmann, T., Hastedt, H., Eilers, M. 2020. Interaction between direct georeferencing, control point configuration and camera self-calibration for RTK-based UAV photogrammetry. The International Archives of the Photogrammetry, *Remote Sensing and Spatial Information Sciences*, 43, 485-492.

Rone W, Ben-Tzvi P 2013. Mapping, localization and motion planning in mobile multi-robotic systems. *Robotica* 31(1):1–23.

Scaramuzza, D.,Fraundorfer, F. 2011. Visual odometry [tutorial]. *IEEE robotics & automation magazine*, 18(4), 80-92.

Štroner, M., Urban, R., Seidl, J., Reindl, T., Brouček, J. 2021. "Photogrammetry using UAV-mounted GNSS RTK: Georeferencing strategies without GCPs." *Remote Sensing*, 13(7), 1336.

Teppati Losè, L., Chiabrando, F., Giulio Tonolo, F. 2020. "Boosting the timeliness of UAV large scale mapping. Direct georeferencing approaches: Operational strategies and best practices." *ISPRS International Journal of Geo-Information*, 9(10), 578.

Wang D, Liang H, Zhu H 2014. A bionic camera-based polarization navigation sensor. *Sensors* 14(7):13006–13023.

Woodman OJ 2007. An introduction to inertial navigation. University of Cambridge, *Computer Laboratory, Technical Report (UCAMCL-TR-696)*, ISSN 1476-2986.

Yousif, K., Bab-Hadiashar, A., & Hoseinnezhad, R. 2015. An overview to visual odometry and visual SLAM: Applications to mobile robotics. *Intelligent Industrial Systems*, 1(4), 289-311.